PROGRESS IN COLOR, COLORANTS AND COATINGS

available online @ www.pccc.icrc.ac.ir

Progress in Color Colorants Coating 17 (2024), 145-158

Ministry of Science, Research and Technology
Institute for Color Science & Technology

Effect of Yb–YAG Laser Parameters on the Operating Regime of Plasma Sprayed NiCrAlY Premixed Coatings

M. A. Ali Bash[1*], A. Mezher Resen[1], A. A. Atiyah[2], K. M. Jasim[1]

[1.] Department of Production Engineering and Metallurgy, University of Technology, P.O. Box: 10066, Baghdad, Iraq.

[2.] Department of Materials Engineering, University of Technology, P.O. Box: 10066, Baghdad, Iraq.

ARTICLE INFO

Article history:
Received: 06 Aug 2023
Final Revised: 21 Oct 2023
Accepted: 25 Oct 2023
Available online: 18 Dec 2023

Keywords:
Plasma spraying
Bond coat
Yb:YAG laser
Specific energy
Phases

ABSTRACT

The direct laser melting of plasma sprayed bond coat has the possibility of improving the surface topography and can be done with Yb:YAG laser. In the current paper, laser melting of plasma sprayed coatings of 50 wt. % standard Amdry 963 ($Ni_{24.5}Cr_6Al_{0.4}Y$) and 50 wt. % standard Amdry 9621 ($Ni_{22}Cr_{10}AlY$) was carried out by using 600 W continuous wave Yb:YAG laser. Notably, the obtained melted tracks were investigated from the upper surface plan view and transverse section. The topography, microstructure, phases, hardness, and compositions of the plasma sprayed coatings and laser-remelted tracks were characterized by scanning electron microscopy (SEM), Energy-dispersive X-ray spectroscopy (EDS), X-ray diffraction (XRD), roughness, and microhardness. By controlling the dependent laser variables (power density and interaction time), a different effect can be obtained for the plasma sprayed bond coating (NiCrAlY). Typically, the results obtained show that at low specific energies, four different distinct zones were observed. These specific energies were not sufficient to produce a uniform melting. The MCrAlY coatings remelted with high specific energies were characterized by completely uniform melting and cellular/dendritic microstructures. The melted coatings have high roughness reduction (1.2 μm) and low hardness (275 $HV_{0.5}$) in comparison with plasma-sprayed coatings (10.5 μm) and (315 $HV_{0.5}$) respectively. Prog. Color Colorants Coat. 17 (2024), 145-158© Institute for Color Science and Technology.

1. Introduction

It has been noticed that the performance and or working time of thermal barrier coating may be enhanced considerably by the suitable selection of intermediate bond coat [1, 2]. Similarly, the bond coat which has been produced mainly by thermal plasma spraying is presented to isolate the superalloy substrate from the hot corrosion attack and also to improve bonding between the substrate and top coat zirconia-based ceramic [3, 4]. It has been demonstrated that it is possible to enhance the surface homogeneity of plasma-sprayed coatings by numerous techniques [5, 6]. Furthermore, the surfacing processes have been used in order to enhance the performance of turbine engines to work at higher temperatures [7-9]. In advanced engines, reducing the surface roughness has

*Corresponding author: * maryam.a.alibash@uotechnology.edu.iq

https://doi.org/10.30509/pccc.2023.167180.1240

become increasingly important to improve the reliability of a thermal barrier coating system [10]. Likewise, a dramatic development in the field of surface engineering of gas turbine engines has well progressed during the past three decades. They have relied on laser surface sealing of plasma sprayed yttria partially stabilized zirconia coating [11, 12] and laser melting improvement of intermediate bond coat MCrAlY systems (where M: Ni, Co or Ni, and Co) [13]. Laser processing of materials has a wide range of applications from micro/nanofabrication techniques to surface treatment, structuring, and modification [14, 15]. As the laser-material interaction is such a complicated phenomenon, advances in laser processing applications require the use of precise mathematical models to represent various processes [16]. In laser surface treatment, the laser processing parameters have a substantial impact on the microstructure of treated surfaces, altering their mechanical characteristics dramatically [17].

In modern advanced engines, superalloy has become the backbone for successful operation at higher temperatures, which benefits from the presence of the plasma sprayed top coat ceramic and intermediate coating [18]. During the last seventy years, the advanced materials of turbine blades have developed considerably to withstand the severe combination of stresses at higher temperatures [19, 20]. There is no doubt that achieving further enhancement in high-temperature engines requires the modification of the surfacing of advanced materials processed by plasma spraying [21]. Bond coat alloys deposited mostly by thermal plasma spraying have high oxidation resistance, good diffusion stability with superalloy substrate, adequate mechanical properties, and high thermal shock resistance [22]. That is to say, the operating temperature of the most advanced gas turbine blades may reach 1100 °C [23]. This can be achieved by using the complex thermal barrier coating system that is a combination of the superalloy, bond coat, thermally grown oxide, and top coat zirconia-based ceramics [24]. This complex system of thermal barrier coating was established in order to overcome the problem of spraying the ceramic coating on a superalloy substrate [25]. Therefore, to adjust the problem of different thermal expansion between ceramic coating and substrate in addition to increasing the adhesion, various bond coatings were developed to decrease thermal stresses [26]. Despite this, the density and homogenization of the coatings, as well as the bonding strength between the coating and the substrate produced by manufacturing techniques remain to be further improved [27, 28].

There were considerable researches dealing with improving the bond coat. To give an illustration, Raj et al. [29] have investigated the NiCrAlY bond-coating on Cu-8 (at %) Cr-4Nb under a thermal cycle of the flame of H_2/O_2. The bond coat has shown considerable internal stresses but without failure after 40 cycles. Significantly, a study has been done by Fiedler [30] in order to increase the life cycle of rocket combustion chambers by modifying the standard NiCrAlY bond coat alloy by adding Cu. The presence of Cu in the bond coat was found to have an important advantage in increasing the compatibility between the bond coat/Cu-based substrate. However, this has an impact on improving both the thermal expansion mismatch and adhesion. The advancement of laser processing of materials may extend to the surface properties of plasma-sprayed bond coats to enhance the performance of thermal barrier coatings. The laser interaction with the plasma sprayed coating has been investigated to change the mechanical, physical, and chemical properties [31]. Nearby, the majority of laser processing of thermal barrier coatings (yttria partially stabilized zirconia and MCrAlY) have been employed with high-power CO_2 lasers [32, 33], but the moderate power Yb: YAG lasers have now considered an acceptable tool for modifying thermal barrier coatings [34].

In this study, a premixed $Ni_{24.5}Cr_6Al_{0.4}Y$ (Amdry 963) and $Ni_{22}Cr_{10}Al1Y$ (Amdry 9621) was plasma sprayed on IN 718 substrate. The effect of Yb: YAG solid-state laser on the topography and microstructural features has been investigated. Furthermore, the effect of laser processing parameters on the response of plasma sprayed NiCrAlY coating.

2. Experimental

The standard powder that is used for plasma spraying was a mixture of Amdry 963 an average particle size of about -90+45 μm and Amdry 9621 an average particle size of -90+45 μm (50 % by weight for each powder). As a rebuttal to this point, it could be argued that the average chemical composition of the starting powders and the powder mixture are listed in Table 1. Superalloy Inconel 718 (Ni- 19 wt. % Cr- 17 wt. % Fe-

3 wt. % Mo- 1 wt. % Co- 0.35 wt. % Si- 0.35 wt. % Mn- 008 wt. % C) was used as the substrate for spraying the powder mixture of MCrAlY with the dimension of 25 mm diameter and 3 mm thickness. The thoroughly cleaned samples were shot blasted by alumina prior to plasma spraying to enhance the surface roughness and increase the adhesion between plasma sprayed coating and substrate. Moreover, air plasma spraying was carried out with a 3MB gun. The powder mixture was preheated at 100 °C to enhance the flowability during feeding through a plasma torch. Furthermore, the powder flow rate of 35 g/min was continuously transported to the copper nozzle from the feeder. The final selected processing sheet used after many initial experiments in order to select the reliable plasma spraying variables is listed in Table 2. The average thickness of bond coatings was approximately 110 ± 15 µm.

The current paper indicates that the plasma sprayed coatings were melted by using a high power 600 W continuous wave Yb: YAG laser (operating at a wavelength of 1060 nm) working at 500 W. Accordingly, the samples were remelted under argon shrouding gas at 1 to 3 mm beam diameter, 1.3 to 55 mm/s traverse speed relative to the stationary laser beam. These laser and processing parameters were selected to obtain wide ranges of specific energies and power densities (Table 3).

Table 1: Chemical composition of the AMDRY 963, AMDRY 9621, and powders mixture (wt. %).

Powder type	Cr	Al	Y	Ni
AMDRY 963	24-25	5-7	0.3-0.5	Balance
AMDRY 9621	21-23	9-11	0.8-1.2	Balance
Powder mixture	22.5-24	7-9	0.5-0.8	Balance

Table 2: Plasma spraying parameters for the bond coatings used in this study.

Processing sheet of shot blasted	
Substrate	Shot blasted IN 718
Grit type	Alumina
Blast Pressure	5 bar
Blast distance	110 mm
Processing sheet of plasma spraying of bond coatings	
Variable	Value
Primary gas	Ar
Pressure, bar	8.2
Flow rate, SLPM	46
Secondary gas	H_2
Pressure, bar	4.2
Flow rate, SLPM	9
Current, A, Ampere	500
Voltage (V), Volt	60
Spray distance, mm	130
Angle, %	90°
Carrier gas	Ar
Flowrate, SLPM	14.7
Powder feed rate, g/min	35

Table 3: Laser and processing parameters of Yb: YAG laser used.

Characteristic	Value
wavelength	1060 nm
Mode	TEM_{00}
Power (P)	500 W
Beam diameter (d)	1 to 4 mm
Traverse speed (V)	1.3 to 55 mm/s
Interaction time, t (d/V)	24-333 ms
Power density, P_A ($P/\pi r^2$)	40-637 W/mm^2
Specific energy, S (P/dV)	0.96- 212 J/mm^2

The upper surface plan views of the plasma sprayed coating and laser melted coatings were first characterized without any metallographic preparation by using optical and scanning electron microscopy to determine the topography, porosity, hardness, and cracks. Thus, the samples were also cut perpendicular to the coating thickness to characterize the transverse sections for bonding, chemical analysis, microstructural evaluation, phases, and closed porosity. Besides, the transverse sections were cold-mounted and then ground and polished using the standard procedures. The polished samples were etched with a solution of equal volumes of HCl, H_2SO_4, and HNO_3 (15 ccs for each acid) and 10 mL Glycerol. The average percentage of porosity, as well as the cell size of the microstructure, were identified and measured from scanning electron microscopy micrographs by using Image analysis.

Qualitative and quantitative chemical analyses of as-sprayed and as-sealed coatings were obtained from X-rays emitted from the surface of transverse sections by using an energy-dispersive spectroscopy detector (EDS) equipped with SEM. As has been mentioned, to evaluate the phases presented in the as-sprayed and as-sealed coatings, a Shimadzu X-ray diffractometer with CuKα radiations and secondary graphite crystal monochromatic were used at 40 kV and 40 mA. The interplanar spacings (d) of the bond coat were calculated from the X-ray pattern by using Bragg's law using the known value of the wavelength of copper and the diffracted angles. Thus, the phases were identified from the standard X-ray data files (JCPDS). The roughness of the upper surface plan views of as-sprayed and laser-treated coatings was measured. The central line average (CLA) was performed using roughness tester type TR200. Microhardness of as-sprayed and laser-treated coatings was measured from the polished transverse section using Digital micro Vickers hardness tester TH714. The average of five readings was obtained at 0.5 kg load.

3. Results and Discussion

In order to investigate the effect of laser remelting of plasma sprayed MCrAlY coatings, both plan view and transverse section before laser melting should be evaluated for roughness, porosity, cracks, irregularity, hardness, chemical distribution, phases, and microstructural features. Figure 1 shows a typical plan view demonstrating the general appearance of MCrAlY plasma sprayed coating. Accordingly, there is a-uniform-non distribution of porosity together with some unmelted and melted-semi particles. Another key thing to remember is the presence of primary and secondary cracks. Actually, the surface roughness of the MCrAlY coating was determined to be approximately 10.5 ± 0.7 µm. The volume fraction of open porosity is 13.6 % ± 1.3. The microscopic examination of the typical transverse section of the plasma sprayed coating clarifies the absence of most upper surface defects (Figure 2). The coating has a relatively small amount of closed porosity (7 % ± 0.8) and fewer amounts of cracks. Moreover, the reduction of defects with increasing the distance from the outer surface of the plasma sprayed coat down to the substrate suggests the solidification mechanism. It has been suggested that the successive lamella solidified of the liquid droplet have less difference between the real area of contact and the apparent area. The reason for this behavior is related directly to the lower amount of internal oxides, unmelted particles, and entrapped gas. As well as the good mechanical interlocking between the plasma sprayed

NiCrAlY coating and the substrate that outcome from the blasting process. Generating good bonding between plasma-sprayed droplets and the substrate. This is due to the good wettability between plasma sprayed metallic coat and substrate. The wettability arises from sufficient pressure of liquid droplets with the substrate producing high impact.

Similarly, Figure 2 illustrates the complex phases formed due to the rapid solidification of the melted mixed powder during impingement onto the superalloy substrate. There is no doubt that the microstructure consists of simultaneous successive thin layers associated with theplasma spraying solidification mechanism. The microhardness of plasma sprayed coatings was measured to be distributed uniformly within the values of 315 ± 15 $HV_{0.5}$. Again, these values are related to the lower values of unmelted particles and low volume fraction of porosity associated with the plasma sprayed coating that has been investigated.

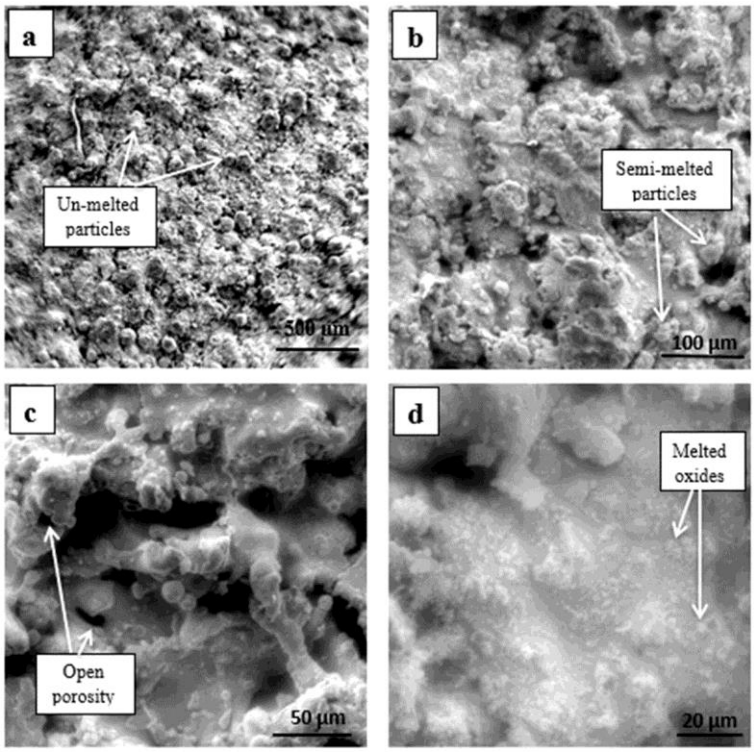

Figure 1: SEM micrograph of the plan view upper surfaces of plasma sprayed bond coat (a) low magnification showing the general appearance, (b) higher magnification showing melted, semi-melted, and unmelted particles (c) and (d) showing the presence of open porosity and oxides as determined from EDS.

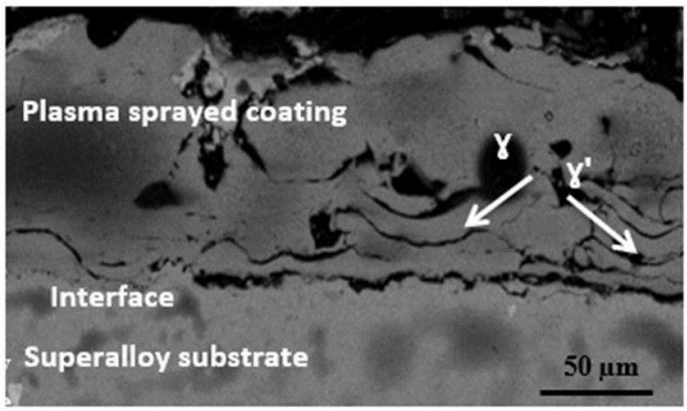

Figure 2: SEM image of the transverse section of plasma sprayed bond coating showing the bonding interface.

They were well established in the literature that laser surface treatments of alloys and sprayed-plasma ceramics are strongly dependent on both power density and interaction time. The relationship between power density and interaction time is known as an operating regime diagram. Unfortunately, there is no such diagram for sprayed-plasma metallic systems; there were established published diagrams for alloys and ceramics [32, 35]. The effect of power, laser beam diameter, and traverse speed on the quality of remelted regions are clearly noticed from optical micrographs at low magnifications.

It has been shown that the combination of power density and interaction time (specific energy = power density x interaction time) plays an important role in the treated zone. The following cases were produced as a result of laser–plasma sprayed NiCrAlY coating interaction. It involves (i) heating effect only, (ii) partial melting at the center of tracks, (iii) uniform melting to a depth of less than 100 μm and (iv) deep melting down to the substrate (Figures 3-6). These four cases were used to establish the operating regime of laser remelting of plasma sprayed metallic (NiCrAlY) coatings (Figure 7). The effect of the wide range of laser processing variables studies showed that high values of power density and interaction time are needed for uniform remelting (Figure 7). It can be seen clearly from the operating regime (Figure 7), the wide band of power density-interaction time for laser remelting of plasma sprayed metallic coatings. The operating regime diagram (Figure 7) suggests that the laser processing of plasma sprayed metallic coatings are not highly sensitive to laser parameter; this is an opposite to operating regime of laser sealing of plasma sprayed ceramics [35]. Therefore, wide spectrums of laser variables can be used to control the good quality of laser remelting of plasma sprayed metallic coatings.

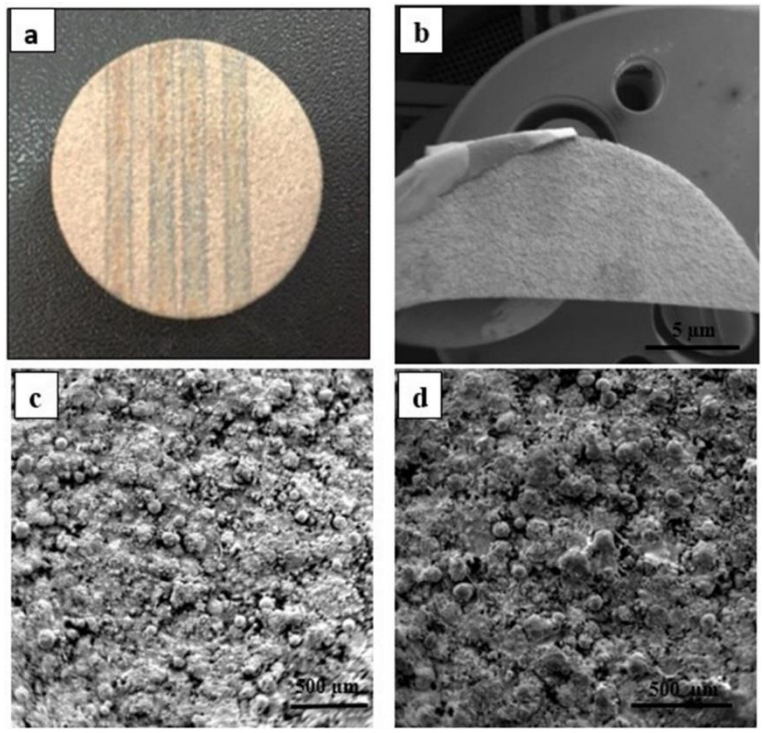

Figure 3: Low magnification photographs of upper surface plan view of plasma sprayed bond coating (a) and (b) at low specific energies showing the only heat effect at different specific energies; from left to right 2.9 to 4 J/mm^2, (c) and (d) SEM at higher magnifications of heating zones.

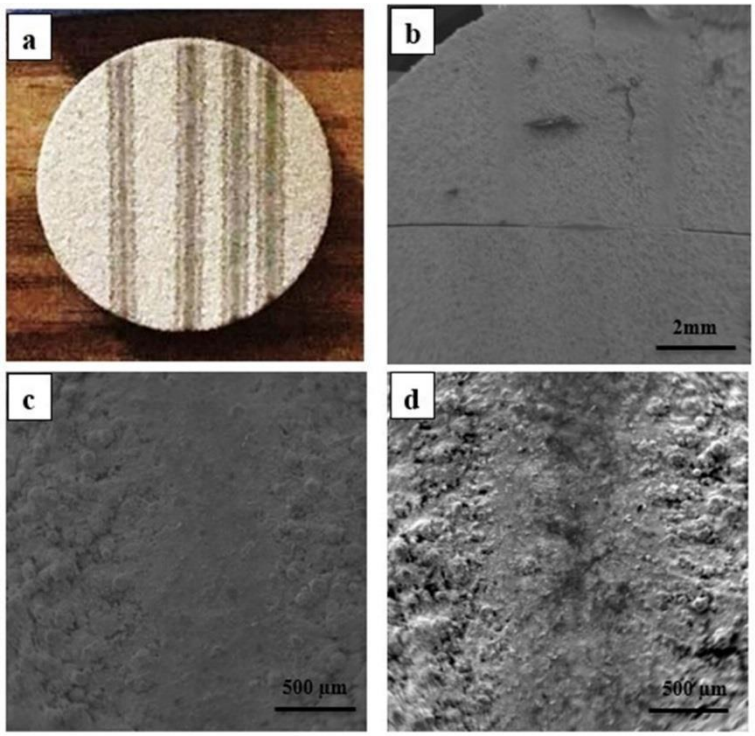

Figure 4: Low magnification photographs of upper surface plan view of plasma sprayed bond coating (a) and (b) at low specific energies showing the partial melting at the center of tracks at different specific energies; from left to right 4.3 to 5.3 J/mm^2, (c) and (d) SEM at higher magnifications of partial melting zones.

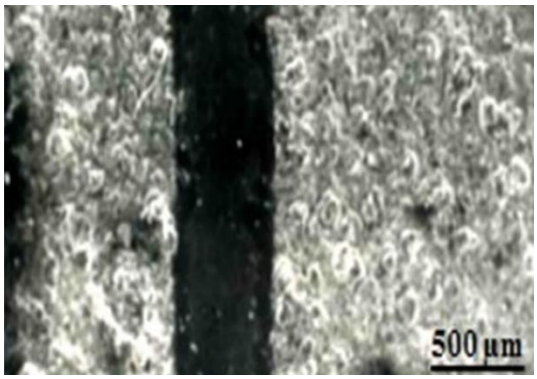

Figure 5: SEM micrograph showing the uniform complete melting of plasma sprayed MCrAlY coating to a depth of 80 % of the plasma sprayed thickness at a specific energy of 15.9 J/mm^2.

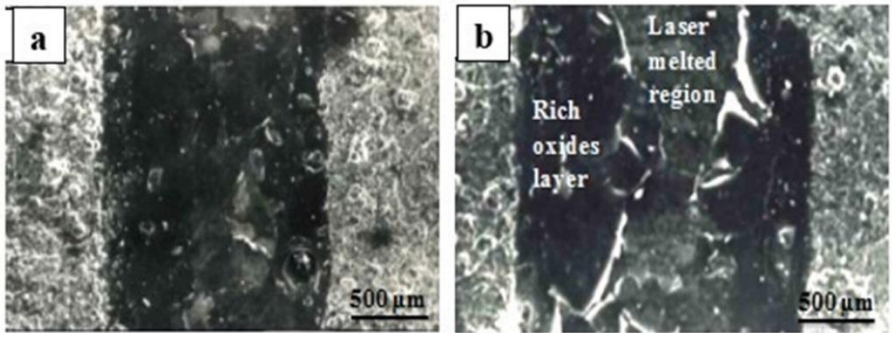

Figure 6: SEM micrographs for plan view of complete melting of plasma sprayed bond coats down to substrate showing the formation of the thin oxide layer at a different specific energy (a) 20.4 J/mm^2 and (b) 82.7 J/mm^2.

It has been shown that at lower power densities, the laser processing parameters were not sufficient for the complete melting of plasma-sprayed coatings. In general, at power density lower than approximately 71 W/mm^2, no effective melting was achieved at interaction time lower than 0.15 s (i.e. approximately 3 to 11 J/mm^2 specific energy) (Figure 3). This specific energy is much higher than those needed for laser sealing of plasma sprayed ceramics and lower than those required for the laser melting of alloys [35]. Completely melted plasma sprayed coatings down to the substrate or melting part of the bond coating were produced at a power density of approximately higher than 71 and lower than 637 W/mm^2 at wide ranges of interaction times (Figure 7).

The specific energies of laser melting were found to be more than 25 J/mm^2 and less than 88 J/mm^2 (Figure 6). At intermediate power densities and specific energies are of approximately 159 to 637 W/mm^2 and 15 to 25 J/mm^2, respectively, only narrow local melting were observed (Figure 4). The upper surface plan views of laser partial melting of plasma sprayed coatings showed different features of structures at different regions corresponding to the Gaussian laser beam distribution (TEM_{00}) used (Figure 8). Four different distinguish zones have been observed. The first zone is the complete melting of the plasma sprayed coating corresponding to the higher energy distribution at the center of the Gaussian distribution of the laser beam (Figure 8). This zone was measured to be approximately equal to a quarter of the treated zone. The second zone at the left and right of the first zone is the non-complete melting (Figure 8). Very narrow zone characterized by low noticeable roughness and fine topography was produced adjacent to the second zone (for both sides) (Figure 8). The fourth zone is the plasma sprayed heat affected zone. It is characterized by fine longitudinal cracks and a structure similar to the plasma sprayed coating.

The cooling rate of the laser melting of plasma sprayed bond coatings was estimated by using the formula reported previously [36] ($\lambda = B\ \varepsilon^{-n}$, where λ is the distance between the second branched crystal arms, ε is the cooling rate, B and n are material constants, B = 40 µm (Ks^{-1}) and n = 0.62) to be 10^3 to 10^4 K/s at higher specific energies more than 25 J/mm^2 (Figure 9). The cooling rate for lower specific energies (15 to 25 J/mm^2) is believed to be higher than 10^4 K/s. It is not determined due to the difficulty of observing the secondary dendrite spacing from the upper surfaces. The absence of secondary arm spacing may suggest the severe cooling rate producing planner solidification. These four zones produced after laser melting have a considerable difference in roughness (Figure 10). The highest reduction in roughness was observed for complete melting zone 1 (1.2 ± 0.5 µm CLA). The roughness increases towards the sides until it reaches its highest value in the fourth zone (plasma sprayed coatings) to be (10.5 µm).

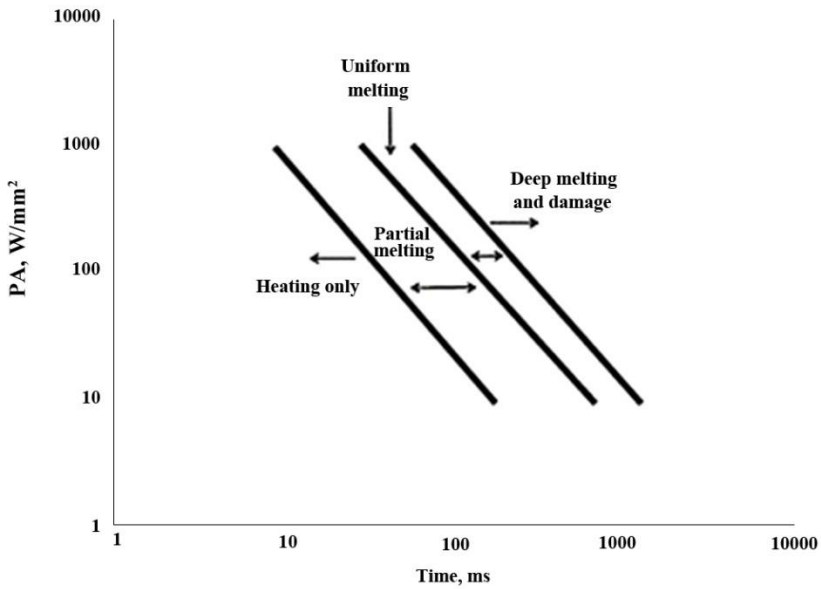

Figure 7: Operating regime of plasma sprayed NiCrAlY coatings.

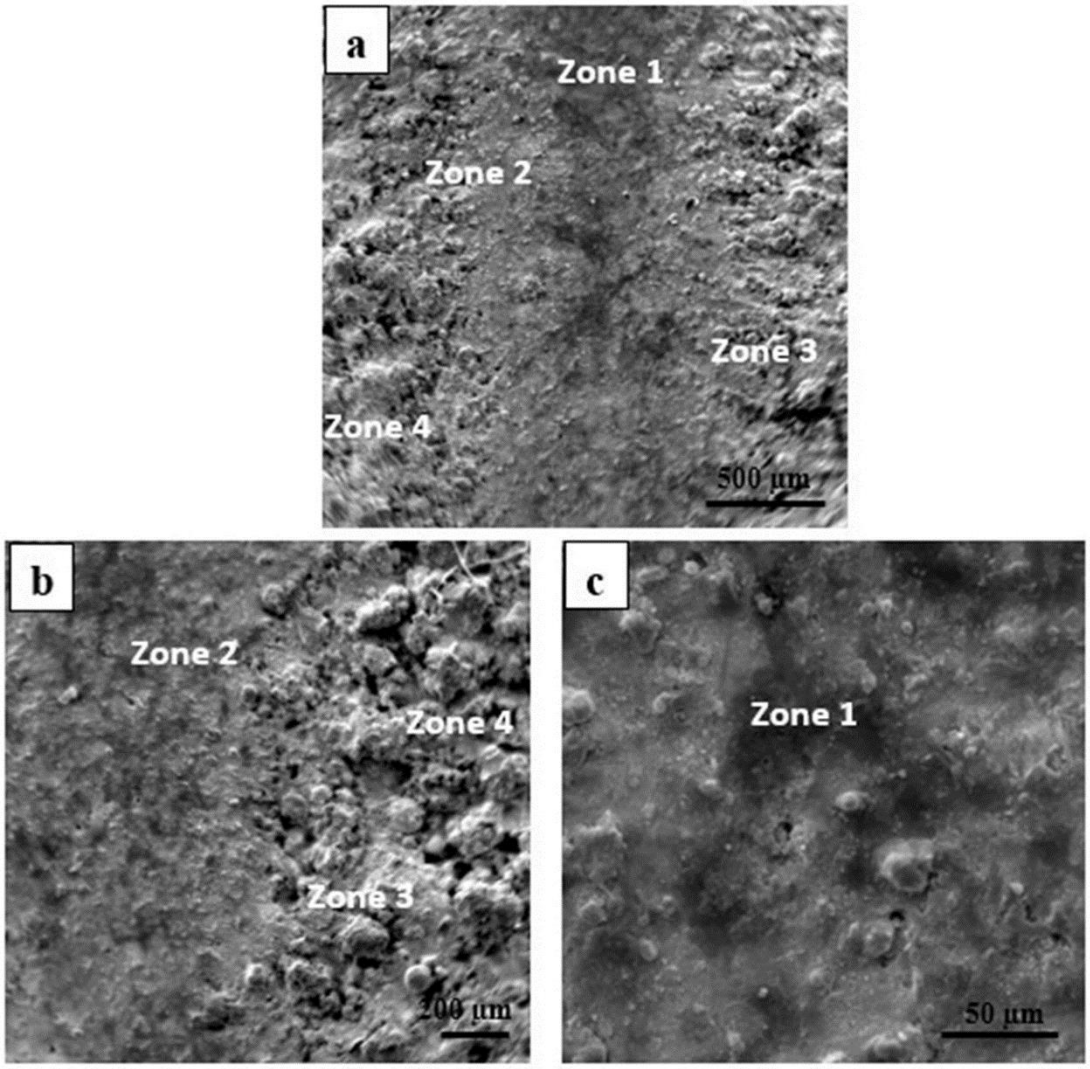

Figure 8: SEM micrograph of the plan view of partial melting of plasma sprayed bond processed at 4.3 J/mm^2 specific energy showing the formation of four zones (a) low magnification, (b) and (c) higher magnifications.

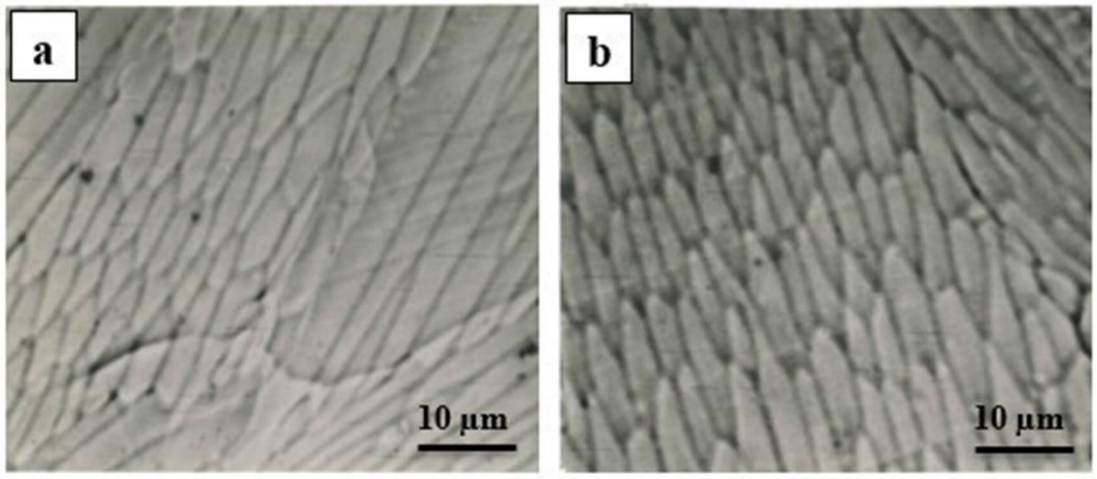

Figure 9: SEM micrograph of the plan view showing the secondary dendrite arm spacing at different specific energies (a) 10.3 J/mm^2 and (b) 15.9 J/mm^2.

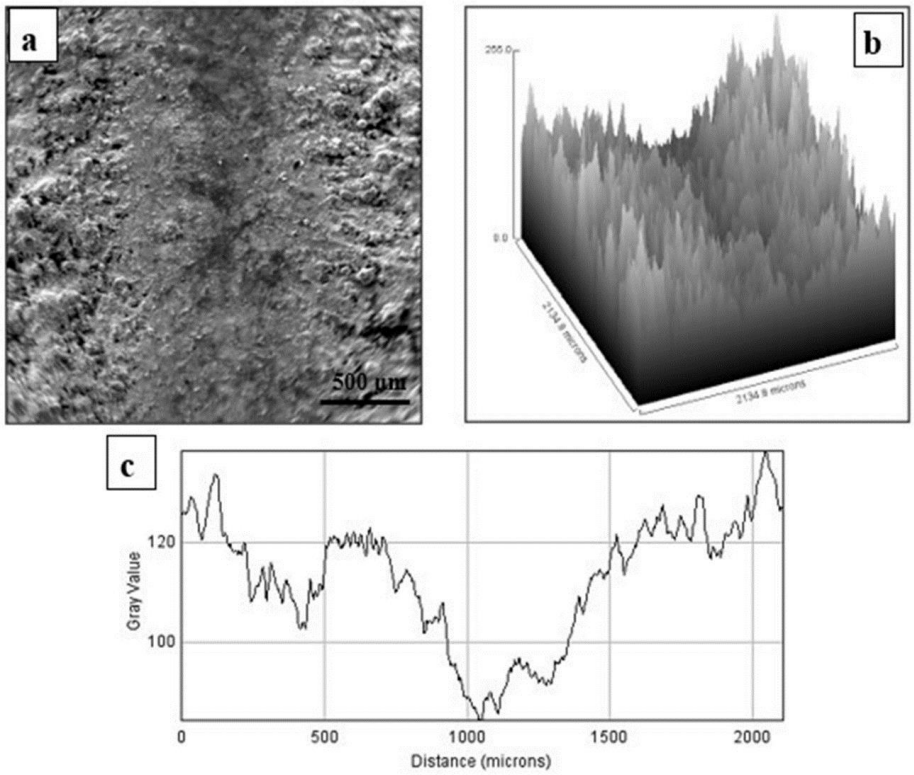

Figure 10: SEM micrograph of an upper surface plan view of partial laser melted coating (a) showing the low roughness distribution of the melted region compared with plasma sprayed coating (b), and (c) surface profile using image J analysis.

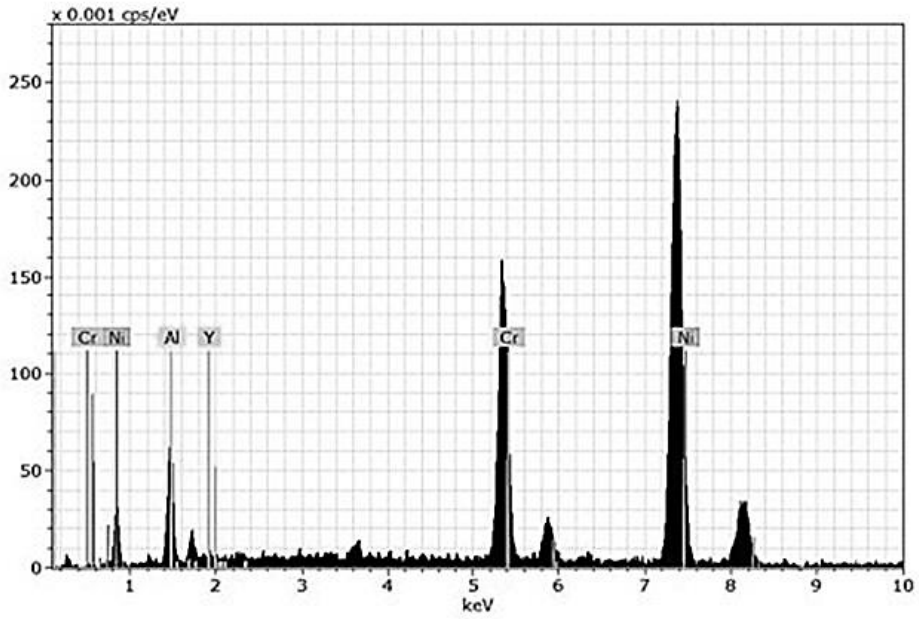

Figure 11: EDS analysis of the bond coating showing the element distribution.

Metallographic observations and EDS analysis of upper surface plan views show the uniform distribution of elements due to the complete melting of powders during the plasma spraying process (Figure 11). Moreover, the quantitative analysis confirms to relatively smaller amount of Al and Cr and a higher amount of Ni compared with the startling mixture powder. The major phases present in the plasma sprayed coatings were determined from the X-ray pattern to be γ (nickel solid solution)/γ'-Ni_3Al and β (NiAl)

intermetallic phase (Figure 12). The other very small amount of minor phases of α -Al_2O_3 and $YAlO_3$ were not detected from X-ray diffraction (due to low percentages); however, the elemental analysis confirmed their presence.

Complete laser remelting, partial melting and only heating of plasma sprayed coatings revealed the similar major and minor phases formed. It is very important to report that the complete laser remelting of plasma sprayed coatings at higher specific energies produced a thin overlay oxidized layer over the laser melted region (Figure 6). Furthermore, these weakly bonded layers were based on oxides of α-Al_2O_3 and $YAlO_3$ (Figure 13). These layers were characterized by peeling from the underneath solidified region because of the different thermal mismatch characteristics of the two layers. The formation of this brittle layer at the surface of the melted plasma sprayed coatings was due to the relatively low density of aluminum and yttrium. These elements float to the outer free surface which reacts with oxygen. The chemical affinity of aluminum and yttrium to oxygen will form α-Al_2O_3 and $YAlO_3$. The microhardness of laser-melted regions (275 ± 5 $HV_{0.5}$) measured from upper polished surfaces and transverse sections was found to be lower than the hardness of plasma sprayed coatings (315 ± 15 $HV_{0.5}$). This reduction of hardness after laser remelting despite the absence of plasma sprayed defects may be attributed to the lower cooling rate and lower internal stresses after laser remelting.

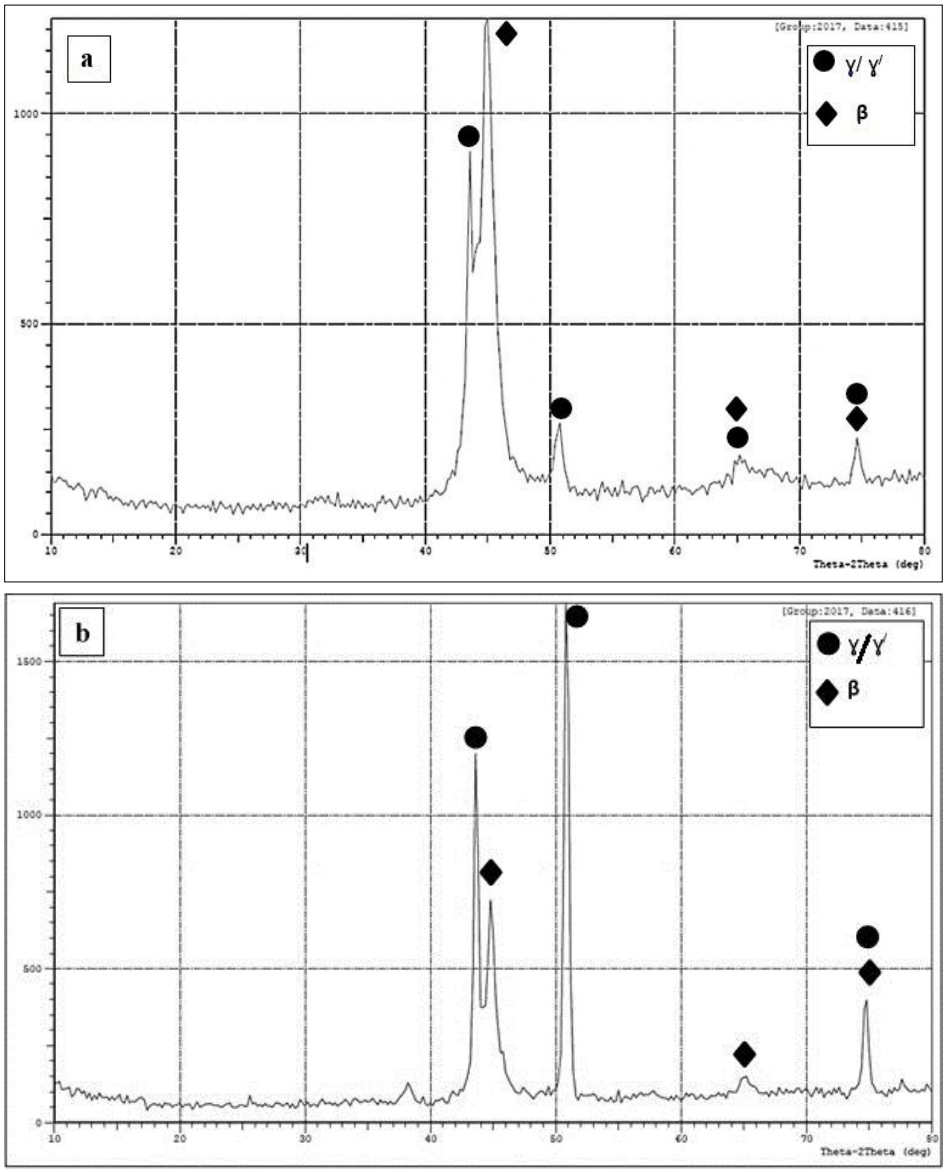

Figure 12: XRD pattern of (a) plasma sprayed coating and (b) laser remelting of plasma sprayed coating.

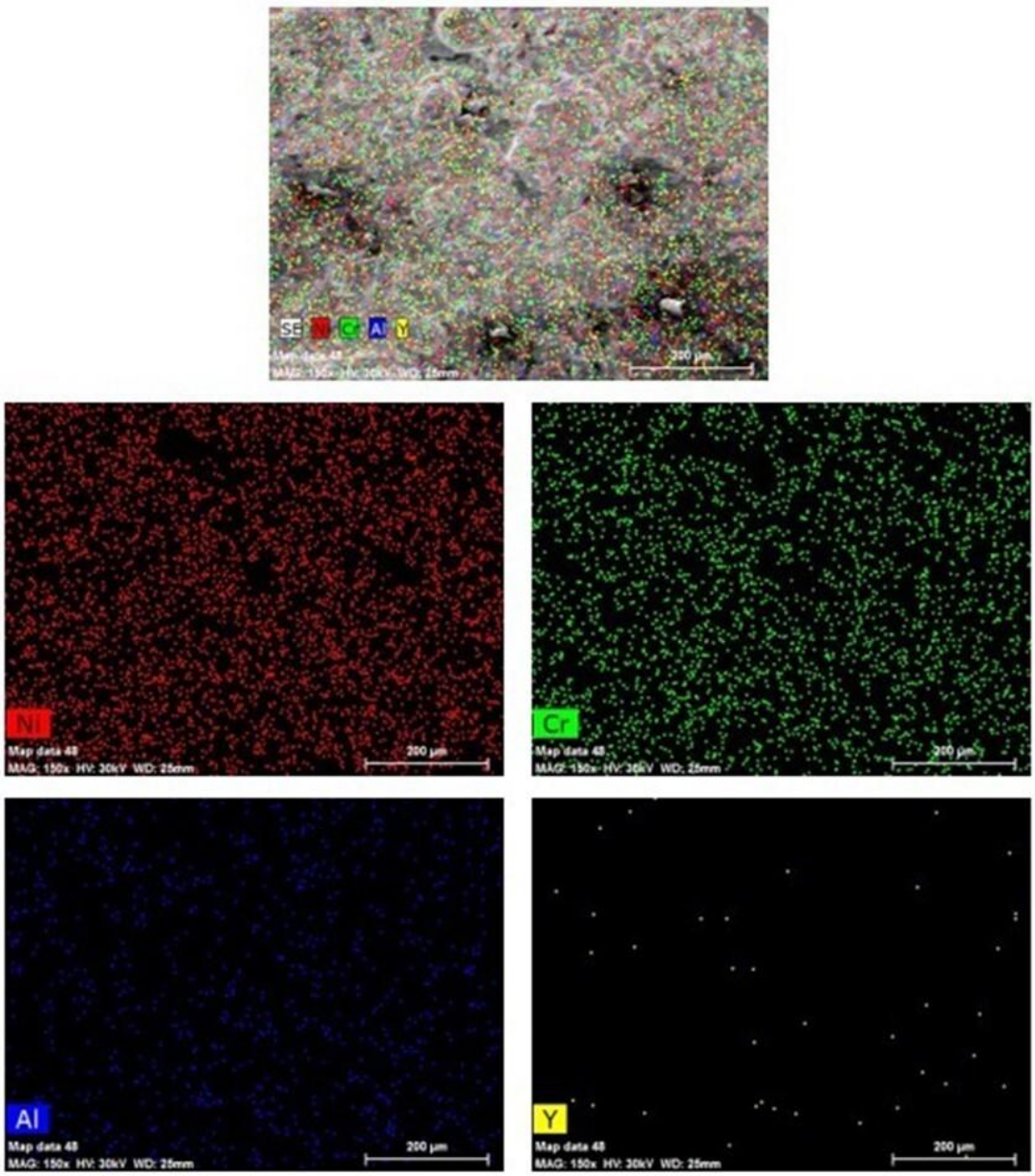

Figure 13: EDS mapping of the upper surface layer of rich oxide after deep laser remelting shows the high percentage distribution of Al and Y.

4. Conclusions

1. The plasma sprayed coatings of a mixed powder of NiCrAlY consist of a homogeneous distribution of ɣ/ɣ' and β phases. The phases do not change after laser remelting under all used dependent parameters.
2. It's possible to produce plasma sprayed NiCrAlY coating surfaces with heating only, partial melting, complete melting, and deep melting depending on the laser-dependent parameters (power density and interaction time).
3. The remelted coatings have a complete melting of a given thickness of plasma sprayed coating dependent on the variables with a uniform distribution of the phases and absence of defects.
4. The roughness of complete laser remelting NiCrAlY coatings was 1.2 µm contrary to 10.5 µm for the plasma sprayed NiCrAlY coatings.
5. The microhardness of the laser remelting zone was 275 HV lower than the microhardness of plasma sprayed coating 315 Hv. Due to the lower cooling rate and internal stresses after laser treatment compared to the plasma spraying process.

5. References

1. Gupta M, Markocsan N, Li X-H, L. stergren O. Influence of bondcoat spray process on lifetime of suspension plasma-sprayed thermal barrier coatings. J Therm Spray Tech, 2018; 27:84-97. https://doi.org/10. 1007/s11666-017-0672-0.
2. Ctibor P, Prantnerová M, Plasma spraying and characterization of chromium carbide-nickel chromium cCoatings. Prog Color Colorant Coat. 2016; 9(2): 281-290.
3. Yamazaki Y, Fukanuma H, Ohno N. Effect of interfacial roughness of bond coat on the residual adhesion strength of a plasma sprayed TBC system after thermal cycle fatigue. J Solid Mechan Mater Eng. 2010; 4(2): 196-207. DOI: 10.1299/jmmp.4.196.
4. Zhao C, Luo L, Xiao C, Zhao X, Wang X, Guo F, Xiao P. The oxidation performance of plasma-sprayed NiAl bond coat: Effect of Hf addition in bond coat and substrate, Surf Coat Technol. 2018; 352(2): 49-58. https://doi.org/10.1016/j.surfcoat.2018. 08.005
5. Garcia-Alonso D, Serres N, Demian C, Costil S, Langlade C, Coddet C. Pre-/during-/post-laser processes to enhance the adhesion and mechanical properties of thermal-sprayed coatings with a reduced environmental impact. J Thermal Spray Technol. 2011; 20(3): 719-735. http://dx.doi.org/10.1007/ s11666-011-9629-x
6. Mei X, Zhang X, Zhang L, Li N, Zhang P, Guo Y, Koval N.N. Enhancing the oxidation resistance of NiCrAlY bond coat by high-current pulsed electron beam irradiation. Coatings 2021; 11: 912. https://doi. org/10.3390/coatings11080912.
7. Clarke D.R, Oechsner M, Padture N.P. Thermal-barrier coatings for more efficient gas-turbine engines, Mater Res Bulletin. 2012; 37:890-941. http://dx.doi. org/10.1557/mrs.2012.232.
8. Abbas RA, Ajeel SA, Ali Bash MA, Kadhim MJ. Optimizing coating thickness of electrophoretic deposition overlay on plasma sprayed YSZ coating using taguchi method. 2022; IOP Conf Ser: Earth Environ Sci. 961 012060. doi:10.1088/1755-1315/961/1/012060.
9. Abbas RA, Ajeel SA, Ali Bash MA, Kadhim MJ. Laser innovation of YSZ electrophoretic deposition overlay on plasma sprayed thermal barrier coating system, Mater Today: Proc. 2022; 57:577-585. https://doi.org/10.1016/j.matpr.2022.01.453
10. Kadhim M.J. Laser cladding of ceramics and laser sealing of plasma sprayed zirconia based thermal barrier coatings, Ph.D. Thesis, Royal School of Mines, Imperial College, University of London, UK, 1990.
11. Bacos MP, Landais D.S, Lavigne O, Mévrel R, Poulain M, Rio C, Vidal-sétif MH. 10 Years activities at onera on advanced thermal barrier coatings. J Aerosp Lab. 2011; 3:1-14.
12. Kadhim MJ. Characterization of laser sealed coatings of yttria partially stabilized zirconia. Optic Laser Eng. 2011;49:785-792. http://dx.doi.org/10.1016/j. optlaseng. 2011.03.008.
13. Luo L, Shan X, Zou Z, Zhao C, Wang X, Zhang A, Zhao X, Guo F, Xiao P. A high performance NiCoCrAlY bond coat manufactured using laser powder deposition. Corr Sci. 2017; 126:356-365. https://doi.org/10.1016/j.corsci.2017.07.018
14. Yang L, Wei J, Ma Z, Song P, Ma J, Zhao Y, Huang Z, Zhang M, Yang F, Wang X. The fabrication of micro/nano structures by laser machining. Nanomaterials. 2019; 9: 1789. doi:10.3390/ nano9121789.
15. Kadhim MJ, Atiyah AA, Ali Bash MA. In-situ laser pelletization of advanced ternary thermal barrier coating system. Mater Res Express. 2019; 6: 035512. http://doi.org/10.1088/2053-1591/aaf65a.
16. Nan L, Li W, Zhang K. Modeling for laser- material interaction to predict and control the cross sectional area of coaxial laser cladding with powder. Proceedings of the International Conference on Advanced Design and Manufacture. 2006.
17. Zhao Y, He W, Du H and Luo P. The effect of laser power on the interface microstructure of a laser remelting nano-SiC modified Fe-based Ni/WC composite coating. Coatings. 2018; 8: 297. doi:10.3390/coatings8090297.
18. Akca E, Gursel A. A review on superalloys and IN718 nickel-based INCONEL superalloy. Period Eng Natural Sci. 2015; 3:15-27. http://dx.doi.org/10. 21533/pen.v3i1.43.
19. Jiang K, Liu S, Wang X. Phase stability and thermal conductivity of nanostructured tetragonal yttria-stabilized zirconia thermal barrier coatings deposited by air-plasma spraying. Ceram Intern. 2017; 43:12633-12640. http://dx.doi.org/10.1016%2Fj.ceramint.2017.06.142.
20. Zoei MS, Sadeghi MH, Salehi M. Effect of grinding parameters on the fracture toughness of WC–10Co–4Cr coating deposited by HVOF. Prog Color Colorant Coat. 2019; 12: 231-239.
21. Oerlikon metco. An Introduction to Thermal Spray, Issue 6 July 2016.
22. Muktinutalapati NR. Materials for gas turbines- An overview. Adv Gas Turbine Technol. 2011; 4: 293-315. http://doi.org/10.5772/20730.
23. Kobylańska–Szkaradek K. Thermal barrier ZrO_2-Y_2O_3 obtained by plasma spraying method and laser melting. J Achiev Mater Manuf Eng. 2006; 17: 77-80.
24. Wang Y, Li J, Liu H, Weng Y. Study on thermal resistance performance of 8YSZ thermal barrier coatings. Inter J Thermal Sci. 2017; 122:12-25. http://dx.doi.org/10.1016/j.ijthermalsci.2017.08.006.
25. Lu Z, Myoung S, Jung Y, Balakrishnan G, Lee J, Paik U. Thermal fatigue behavior of air-Plasma sprayed thermal barrier coating with bond coat species in cyclic thermal exposure. Materials. 2013;

6:3387-3403. https://doi.org/10.3390/ma6083387.
26. Hemker KJ, Mendis BG, Eberl C. Characterizing the microstructure and mechanical behavior of a two-phase NiCoCrAlY bond coat for thermal barrier systems. Mater Sci Eng A. 2008; 483-484:727-730. http://dx.doi.org/10.1016/j.msea.2006.12.169.
27. Zhang YP, Zhou ZR, Cheng JM, Ge Y, Ma H. Laser remelting of NiCoCrA1Y clad coating on superalloy. Surf Coat Technol. 1996; 79: 131-134. https://doi.org/10.1016/0257-8972(95)02448-4.
28. Ali Bash MA, Mezher Resen A, A. Kareem AH, Muhi Abdulsahib Y. Improving the hot corrosion behavior of plasma-sprayed MCrAlY by RF sputtering of TiO_2 nanocoating and laser remelting treatment. Prog Color Colorants Coat. 2024; 17(1): 27-38. https://doi.org/10.30509/pccc.2023.167142. 1221.
29. Raj SV, Ghosn LJ, Robinson C, Humphrey D. High heat flux exposures of coated GRCop-84 substrates. Mater Sci Eng A. 2007; 457: 300-312. http://dx.doi. org/10.1016/j.msea.2006.12.133.
30. Fiedler T, Fedorova T, Rösler J, Bäker M, Design of a nickel-based bond-coat alloy for thermal barrier coatings on copper substrates. Metals. 2014; 4:503-518. https://doi.org/10.3390/met4040503.
31. Sidhu BS, Puri D, Prakash S. Characterisations of plasma sprayed and laser remelted NiCrAlY bond coats and Ni3Al coatings on boiler tube steels. Mater Sci Eng A. 2004; 368:149-158. http://dx.doi.org/10.1016/j.msea.2003.10.281.
32. Kadhim MJ, Rawlings RD, West DRF. Operating regimes for laser surface engineering of ceramics. J Mater Sci. 1992; 27:1927-1936. https://ui.adsabs. harvard.edu/link_gateway/1992JMatS..27.1937J/doi: 10.1007/BF01107223.
33. Utu D, Marginean G, Serban V, Codrean C. Corrosion behavior of laser remelted CoNiCrAlY based composite coatings. Engineering. 2010; 2:322-327. http://dx.doi.org/10.4236/eng.2010.25042.
34. Ali Bash MA. Optimizing, phase transformation and hot corrosion resistance of laser sealing plasma sprayed ceria stabilized zirconia thermal barrier coatings, Ph.D. Thesis, Department of Production Engineering and Metallurgy, University of Technology, Baghdad, Iraq, 2017.
35. Majumdar J, Manna I. Laser processing of materials. Sdhana. 2003; 28:495-562. http://dx.doi.org/10. 1007/BF02706446.
36. Baesloki WA, Weeter L, Krishnamurphy S, Smith P, Materials Research Society. Symposium Proceeding, 1984; 28:375.

How to cite this article:
Ali Bash MA, Mezher Resen A, Atiyah AA, Jasim KM. Effect of Yb-YAG Laser Parameters on the Operating Regime of Plasma Sprayed NiCrAlY Premixed Coatings. Prog Color Colorants Coat. 2024;17(2):145-158. https://doi.org/10.30509/pccc.2023.167180.1240.